Two-Dimensional Maxwell Fisheye for Integrated Optics

O. Bitton,[1] R. Bruch,[2] and U. Leonhardt[2,*]

[1] *Chemical Research Support Department, Weizmann Institute of Science, Rehovot, Israel*

[2] *Department of Physics of Complex Systems, Weizmann Institute of Science, Rehovot, Israel*

(Received 1 March 2018; revised manuscript received 10 June 2018; published 25 October 2018)

Maxwell invented a refractive-index profile where light goes in circles and every point is focused. A device with such a profile is called the Maxwell fisheye and it is an absolute optical instrument: it has the ability to collect all rays from any emitting source and recombine them in phase at the corresponding focal point inside the device. Absolute optical instruments may find diverse applications if they can be made in integrated optics on a silicon chip for infrared light. We have fabricated the Maxwell fisheye in silicon photonics and have demonstrated its focusing properties. Our fabrication technique can also be applied to the manufacturing of other devices where smooth and sharp structures need to be made in one lithography step.

DOI: 10.1103/PhysRevApplied.10.044059

I. INTRODUCTION

The usage of miniaturized devices for telecommunication systems continues to grow and has greatly attracted researchers and development engineers due to their wide applications. Miniaturized devices—optical couplers, connectors, beam collimators, beam splitters, etc.—use the integration of micro-optical components such as ball lenses and gradient-index lenses [1,2]. However, the performance of conventional micro-optical components is limited mainly by aberration due to off-axis skew rays. On the other hand, spherical-gradient refractive-index (GRIN) lenses, the index profiles of which are radially symmetric, have no optical axis and therefore are free of off-axis skew rays. The subject of GRIN media [3] dates back to the mid-19th century [4,5] and, more recently, has drawn much attention, because of their utility for various imaging functionalities [6–13]. The earliest GRIN lens is a spherically symmetric lens, the Maxwell fisheye (MFE) [4,5,14]. The MFE lens is an absolute optical instrument [15,16], designed to provide perfect point-to-point imaging within the lens. It can be applied for perfect imaging [6] under certain conditions [17,18], but also for on-chip optical communication free of aberrations and cross talk, and may exhibit interesting quantum effects [19].

Three-dimensional (3D) MFE lenses were first made in 1986 by the use of a modified suspension polymerization technique [20–22]. Ilyas and Gal fabricated the conventional parabolic GRIN planar microlens in silicon using porous silicon [23]. MFE lenses have been fabricated on optical glasses using the ion-exchange method [24] and by liquid droplets [9]. Two-dimensional (2D) MFE lenses are particularly attractive since they can be used for integrated optics on a silicon chip for telecommunication wavelengths (infrared light) or with gallium nitride or diamond integrated optics for visible light. Such a lens has been made with dielectric nanostructures in silicon photonics [25] but did not show the desired imaging properties of a MFE lens due to backscattering on the nanostructures.

Here, we report on the fabrication of a MFE of unprecedented quality, made of a pure planar waveguide in silicon, and demonstrate its focusing properties. The key to the high quality of our MFE is the fabrication of smooth and sharp structures in one lithography and etching step, an achievement that is demonstrated in detail in this paper. Our technique can also be applied to the fabrication of other devices where smooth and sharp structures need to be combined. In particular, it enables the implementation of conformal-transformation optics [25–27] in silicon photonics. There, variations in the height of the waveguide may give rise to the required refractive-index distributions [28] and Bragg mirrors may serve as reflectors. The simplest application of transformation optics is in adapting the shape of optical devices to requirements different from optics, for example, to constraints set by electronic functionalities. Reshaping also provides recipes for invisibility [29] and illusion optics [30]. Other more sophisticated applications [27] include the multiplication or combination of sources for lighting, the sharp bending of waveguides without causing significant loss, the facilitation of highly directional radiation, and nearly perfect cloaking [31].

In 1854, Maxwell considered a spherically symmetric lens of infinite size with a refractive-index profile

*ulf.leonhardt@weizmann.ac.il

that focuses light rays coming from any point to a corresponding image point [5]. The profile of the index of refraction is rotationally symmetric and follows the simple formula

$$n(r) = \frac{2n_0}{1 + (r/a_0)^2}. \quad (1)$$

Here, r is the distance from the center of the lens, n_0 denotes an ambient refractive index, and the constant a_0 sets the length scale of the profile. Maxwell showed two remarkable properties of this—by then hypothetical—device: light rays follow circular paths and all points are imaged into corresponding focal points. Luneburg [32] discovered that the unusual imaging properties of the MFE have a geometric interpretation: the device is performing a stereographic projection from the surface of a sphere [Fig. 1(a)] to a plane [Fig. 1(b)]. One can easily see that a circle on the sphere is mapped to another circle on the plane [33], which explains why light goes in circles in Maxwell's lens. On the sphere, all light rays emitted from an arbitrary point meet at the corresponding antipodal point [Fig. 1(a)], so in the plane each point of emission comes to a perfect focus at the projected antipodal point, which explains why the MFE lens is an absolute optical instrument [15]. In practice, the MFE lens should be surrounded by a mirror [6] at radius a_0, in order to confine the index range between n_0 and $2n_0$, without affecting the defining imaging properties of the absolute optical instrument [6,15].

Since 2009, the subject of the Maxwell fisheye has enjoyed a renaissance in connection with the tantalizing prospect of perfect imaging without negative refraction [6] that has been subject to much debate [34]. It has been experimentally demonstrated using microwaves [35] but was only fully theoretically understood in 2015 [17,18]. It turns out that imaging with subwavelength resolution is only possible at certain resonance frequencies, which requires a sufficiently high fabrication quality. Here, we report on a high-quality MFE lens made without the use of nanostructures (that may cause artifacts [25]). We have not demonstrated the subwavelength resolution yet but we have seen the correct focusing properties of Maxwell's device [5].

We make 2D MFE lenses on a silicon chip, which are engineered for a wavelength of 1550 nm. The device consists of a source, used to couple waves in, an outlet for decoupling waves from the device, and a Bragg reflector, the surrounding mirror [Fig. 1(c)]. The propagating modes designed to follow the effective index profile of Eq. (1) are calculated to be polarized such that the electric field points in the plane of the device and is transversal to the direction of propagation (the field is E polarized, which is often called TE polarized, although the terminology is confusing [36]). By using gray-scale electron-beam lithography (EBL), we fabricate a gradual silicon structure that is engineered to simulate the profile of index of refraction and accordingly mimic the virtual MFE sphere. A similar technique has been used for the fabrication of the Luneburg lens [11] and a simple version was used to make crude Maxwell and Eaton lenses [9]. However, we also need to fabricate the Bragg mirror, adjacent to the lens, which consists of alternating vertical silicon thin walls separated by thin air gaps, around the smoothly curved silicon. The challenge is to combine the etching of the smooth profile and the sharp structures of the Bragg mirror in a single lithography and etching step. The Bragg structures and the smooth profile are characterized by a different type of curvature (anisotropic) compared to that of the MFE (isotropic), which normally require different etching techniques. In the previous work [25] on making a MFE in silicon photonics, only sharp structures were made, as the smooth refractive-index profile was approximated by sharp silicon pillars. Our technique allows us to fabricate a MFE without the artifacts caused by such dielectric nanostructures [25].

II. DESIGN

Our device [Fig. 1(c)] consists of layers of silica (SiO_2) and silicon on a silicon substrate, covered by a thin protective layer of poly(methyl methacrylate) (PMMA). These layers form a planar waveguide where the height h of the silicon layer is made to vary as the result of our fabrication technique. In this section, we describe how the varying height of the silicon layer gives rise to an effective refractive-index profile. The relationship between the height and the refractive index is then used to implement the profile of the Maxwell fisheye, given in Eq. (1), as a height profile [Fig. 2(a)].

The desired refractive-index profile of Eq. (1) varies on much longer length scales a_0 than the wavelength λ, so the height profile must vary on longer-than-wavelength scales as well. In order to find the translation between the height and the index, we therefore assume that the layers are perfectly planar; h does not vary at all in this step. The silica layer is thick compared with the wavelength, so for the design of the waveguide we assume it to be infinitely extended. Effectively, we are dealing with four regions depending on the vertical coordinate z that is normal to the layers: (1) $z < -h/2$ bulk silica with refractive index n_s, (2) $-h/2 < z < h/2$ silicon with index n_{Si}, (3) $h/2 < z < h/2 + h_p$ PMMA with index n_p, and finally (4) air with refractive index $n = 1$.

In order to calculate the effective refractive index depending on the silicon height h, we decompose the electromagnetic field into modes that are plane waves orthogonal to the z direction. We set the system of coordinates such that the light propagates in the x direction. The electric-field strength points in the y direction, orthogonal to the light propagation and parallel to the planar device. We describe the monochromatic electric-field amplitude E,

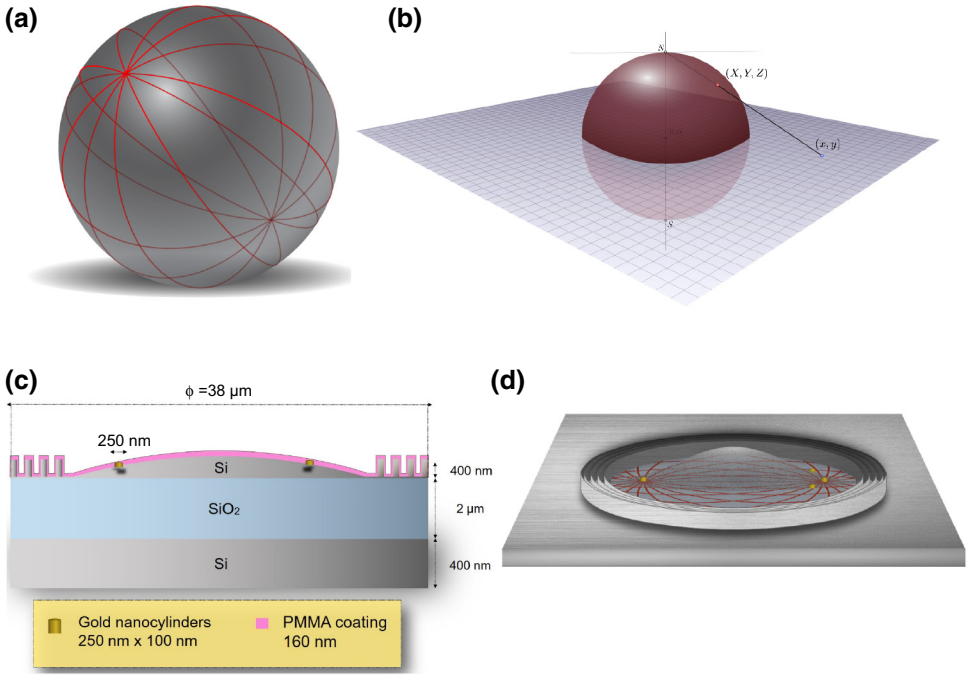

FIG. 1. The Maxwell fisheye. (a) Light propagates in circles on the surface of a virtual sphere. (b) The principle of stereographic projection of the Maxwell fisheye lens shown in (a). A plane cuts the sphere at its center; a line is drawn from the north pole through any point on the surface of the sphere and intersects this plane at another point, the projected point. The south pole is projected onto the center of the sphere and the north pole to infinity. (c) A cross section of the 2D Maxwell fisheye lens in silicon. (d) Light propagation in the 2D Maxwell fisheye lens. The red curves show the ray trajectories.

satisfying the Helmholtz equation, as $E = \psi_j(z)\exp(i\beta x)$, where β denotes the wave number in the propagation direction. We write, for the four regions,

$$\begin{aligned}
\psi_1 &= a_1 e^{\sqrt{\beta^2+n_s^2k^2}z},\\
\psi_2 &= \cos\left(\sqrt{n_{\mathrm{Si}}^2k^2-\beta^2}z\right)+a_2\sin\left(\sqrt{n_{\mathrm{Si}}^2k^2-\beta^2}z\right),\\
\psi_3 &= a_3 e^{\sqrt{\beta^2+n_p^2k^2}z}+a_4 e^{-\sqrt{\beta^2+n_p^2k^2}z},\\
\psi_4 &= a_5 e^{-\sqrt{\beta^2+k^2}z},
\end{aligned} \tag{2}$$

where $k = 2\pi/\lambda$ with $\lambda = 1.55$ μm. We take the refractive indices of the materials from the literature [37–39] and put $h_p = 60$ nm. We require that both ψ and $\partial\psi/\partial z$ are continuous across the interfaces of the layers and solve numerically the resulting six equations for the five unknown coefficients a_m and the lowest β, depending on the height h, which we vary from 50 nm to 400 nm. The effective refractive index n is then given by β/k. Inverting numerically the height dependence of n and using Eq. (1) for n, we obtain the required height profile of the Maxwell fisheye [Fig. 2(a)] that needs to be fabricated.

III. FABRICATION

We fabricate the fisheye lens on a silicon-on-insulator (SOI) substrate with a top silicon thickness of 400 nm and an SiO_2 thickness of 2 μm using gray-scale electron-beam lithography (EBL). Figure 2(a) shows the radial height curve of the Si layer that corresponds to the effective refractive-index profile of the Maxwell fisheye, Eq. (1), determined with the method described in Sec. II. Figure 2(a) also shows the atomic-force-microscope (AFM) data of an actual device, proving that our fabrication method meets its goal.

The details of the fabrication method are absolutely crucial in order to be able to etch both the gradual height profile and the deep trenches of the Bragg mirror within the same etching step. However, as these are just details, we describe them in the Appendix. Here, we give only an overview of the main steps involved. We first spin-coat the SOI chip with photoresist, with SU-8 resist turning out to be most suitable. The resist is exposed with an electron beam that cross-links the polymers of the resist depending on the energy dose. Then, a mixture of gases under plasma conditions is applied to etch both the resist and the silicon, where the cross-linked regions of the resist partially protect the silicon and serve as a mask. The result of the etching is measured with an AFM. Significant effort goes into optimizing the etching conditions with regard to the pressure, energies, and flows in the plasma so that the profile in the resist will be transferred efficiently to the Si (see the Appendix). Given the optimal etching process, a contrast curve [Fig. 2(b)] is determined that relates the applied electron-beam (e-beam) dose to the

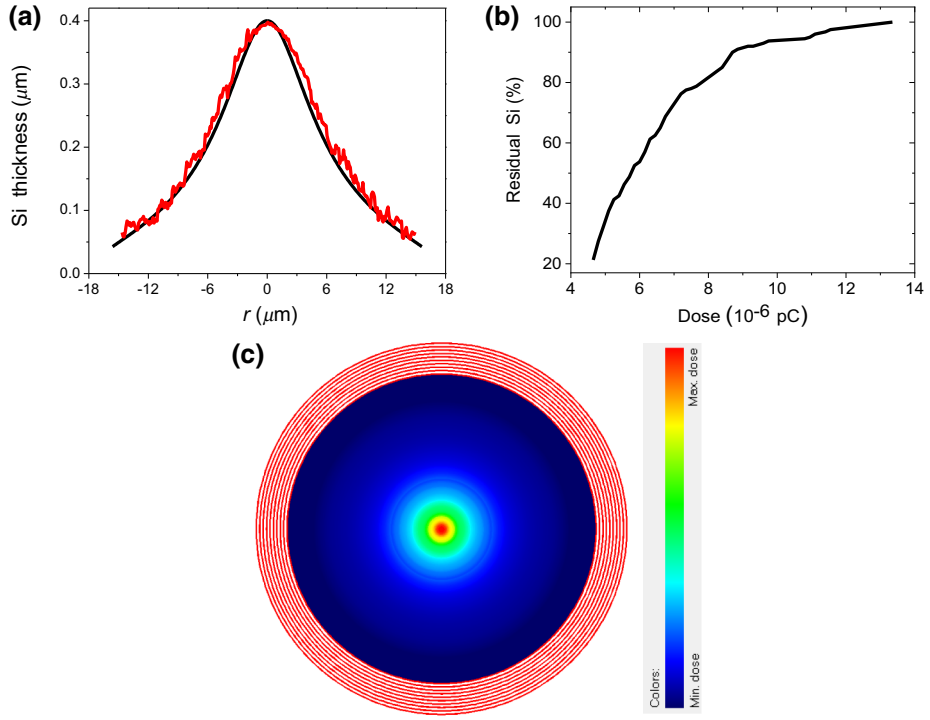

FIG. 2. The design and the actual device. (a) The calculated gradient height of the silicon (black) and the height curve of the actual device measured by atomic force microscopy (red). (b) The contrast curve of the resist and the etching process. The contrast curve is derived after the etching process. (c) The design of the Maxwell fisheye is composed of dots, where each has a different exposure time. The color represents the dose, ranging from a minimum dose of 3.45 pC to a maximum dose of 10.65 pC. The dose distribution takes into account the contrast curve shown in (b). The Bragg mirror is colored in red in order to distinguish it from the gradual profile of the fisheye lens.

height of the silicon. The contrast curve is then applied in determining the energy dose for each pixel in the design, in order to yield the required height profile [Fig. 2(a)]. The obtained profile fits to the simulated curve very nicely [Fig. 2(a)]. The obtained average roughness is 5 nm, with a root-mean-square (rms) roughness of 7 nm.

After the fisheye profile and the Bragg mirror are transferred to the silicon, we use EBL to form gold nanoparticles on the fisheye structure, to serve as the source and outlet to couple the light in and out. One nanoparticle plays the role of the source while three nanoparticles are deposited on the other side of the device, one of them—the receiver—being exactly symmetric from the source, while two other nanoparticles serve as test outlets for verification purposes. The source and outlet nanoparticles have to be of the exact same shape and size in order to fit the ansatz that the source and drain must be accurate copies of each other [18]. By using alignment marks, we expose holes in the PMMA resist with an overlay accuracy of 20 nm. Then we evaporate Cr (2 nm) and Au (100 nm) following a lift-off process that results in cylindrical gold nanoparticles with a diameter of 250 nm and a height of approximately 200 nm. The cylindrical shape allows the generation of the mode for which this MFE-inspired structure was designed. Finally, the substrate is covered with a 60 nm thickness of PMMA for protection. Figure 3 shows images of the fabricated devices.

IV. TESTING

To test the fabrication quality, we take images with a scanning electron microscope (SEM), as shown in Fig. 3. When exciting the left (source) nanoparticle, the *E*-polarization mode should be scattered out of the nanoparticle, coupled into the propagating layer of the device, and focused at the antipodal point. In this case, only the symmetrically deposited nanoparticles should light up while the others remain dark.

To test these optical properties of the MFE lens, we use a setup that both displays the illumination of the device and facilitates the irradiation of the gold nanoparticles [Fig. 4(a)]. As we work with far-infrared light (1.55 μm), a single camera cannot both image the device and irradiate the nanoparticle target. Thus a simple hybrid setup is used with two illumination sources, a red laser (780 nm) combined with the IR laser (1.55 μm), and two cameras with a link between them. The red-laser beam is combined through a dichroic mirror with the IR beam. It serves as a witness on the visible camera to guide the IR beam throughout the sample [cf., Fig 4(a)]. We image

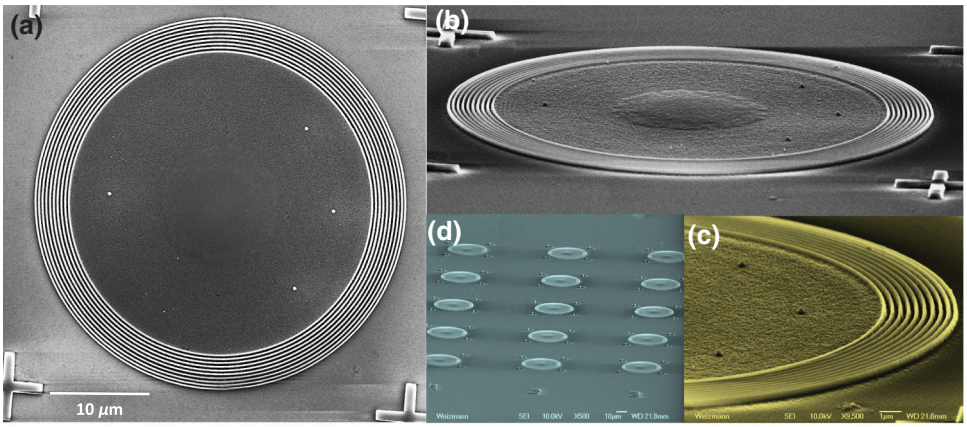

FIG. 3. Scanning electron microscope (SEM) images of the Maxwell fisheye. (a) A SEM image of an MFE composed of circular graded silicon surrounded by a Bragg mirror. (b) A tilted SEM image of the fisheye, scanned at approximately 70°. (c) A magnified tilted SEM image of a fisheye, showing the Bragg mirror and the gold nanoparticles that serve as the outlet points. (d) A low-magnification image showing many fisheyes.

the device with bright-field microscopy and illuminate the nanoparticles down to the diffraction limit of an infrared achromatic Olympus objective.

For more than 25 MFEs, we can see that light is indeed coupled out only at the receiver nanoparticle while the other test nanoparticles remain dark [Fig. 4(b)]. In all cases, the infrared laser is linearly polarized, which should match the *E*-polarization mode (where the electric field is perpendicular to the direction of propagation in the Si layer). The cylindrical nanoparticle should scatter some part of the incident light into this fisheye mode. We observe, however, that despite the cylindrical shape of the nanoparticle, the in-coupling is highly inefficient. We also observe that the in-coupling depends on the polarization, whereas the out-coupled light is unpolarized (as we observe by adding a polarizer before the IR camera). These polarization issues are subject to further investigation.

V. SUMMARY

We design, fabricate, and test a Maxwell fisheye lens on a silicon chip for telecommunication wavelengths. The

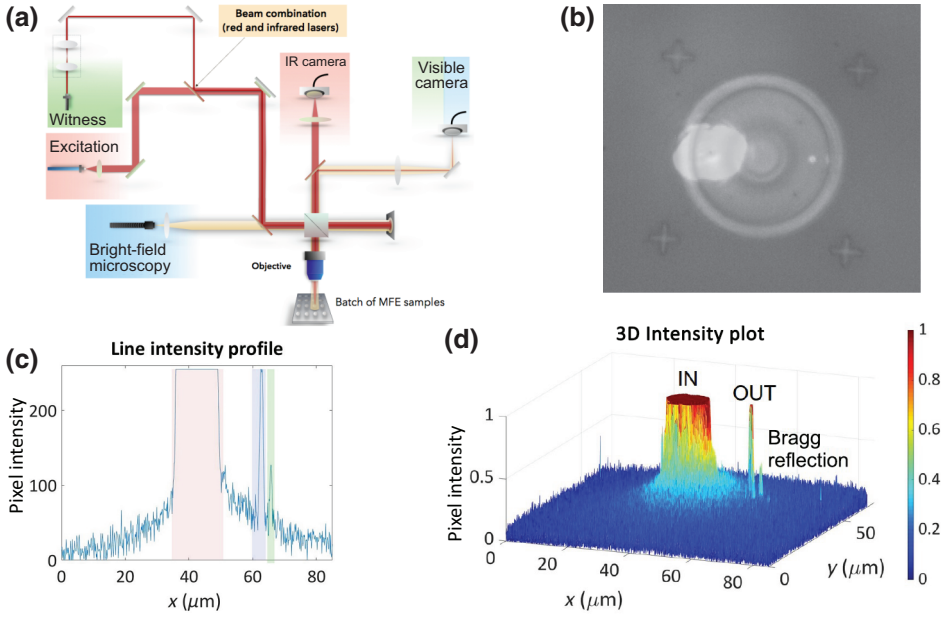

FIG. 4. The measurement setup and results. (a) The optical setup. Light from the excitation laser in the infrared (wavelength 1550 nm) is combined with visible red light (wavelength 750) in order to find the image. (b) Superimposed pictures from the visible camera and the infrared camera. The IR beam is illuminating the left nanoparticle (the source) and the nanoparticle on the right (the outlet) is lighting up after propagation inside the device. (c) The intensity profile on the IR camera, along the diameter of the nanoparticles, showing the focusing effect of the MFE. (d) A 3D plot of the IR camera when hitting the nanoparticle on the left side. A clearly localized peak appears on the right but not on the auxiliary nanoparticles [Fig. 3(a)]. The correct image nanoparticle is thus lighting up after propagation of the coupled light inside the device. The small side peak is probably an artifact of reflection at the Bragg mirror, as shown in (b).

MFE lens is made of planar waveguides surrounded by a Bragg mirror. We succeed in manufacturing such a device in a single etch and lithography step and demonstrate its principal imaging properties. Our fabrication technique is generalizable to other micro-optical components in integrated optics that require both smooth and sharp structures.

ACKNOWLEDGMENTS

We are grateful for illuminating discussions with Guy Bartal, David Lishan, Dan Oron, Sahar Sahebdivan, and Alexander Yoffe. This research was supported by the European Research Council and the Israel Science Foundation, a research grant from Mr. and Mrs. Louis Rosenmayer and from Mr. and Mrs. James Nathan, and the Murray B. Koffler Professorial Chair. O.B. and R.B. contributed equally. O.B fabricated the device, R.B. carried out the experiment, and U.L. designed the device. All of the authors discussed the results and contributed to the writing of the paper.

APPENDIX: FABRICATION DETAILS

We use gray-scale EBL to fabricate both the gradual height profile of the Si layer and the narrow trenches of the Bragg mirror surrounding the device. SU-8 resist is found to be the most suitable for this application for several reasons. First, SU-8 is characterized by a low-contrast curve and therefore enables the modulation of exposure doses to develop the 3D structure. Differential exposure doses lead to multiple heights of cross-linked resists across the surface. Second, SU-8 resist is sensitive to electrons and therefore EBL can be used to enable a very good lateral resolution. The lithography is composed of two steps. First, the shape of the structure is patterned in a SU-8 photoresist layer by the use of gray-scale lithography. Second, the photoresist layer is used as a nested mask (multiple height levels) in dry etching, where the structure is transferred into the silicon substrate to a specified depth corresponding to the height of the desired final structure.

The resist-contrast curve allows us to map the required absorbed energy to the resist thickness. As the etch rates of silicon and SU-8 are different for the same plasma conditions, we construct the contrast curve to be based on the etching procedure. For each dose value, we correlate a residual Si thickness after the dry etching process.

In order to extract the contrast curve, at a 500-nm thickness of SU-8 resist on an SOI substrate, we expose small features by EBL (Raith, *e − linePlus*) using 30 kV and a 10 μm aperture size, yielding an *e*-beam current of 30 pA. The write field size is 100 μm. Both for the contrast-curve extraction and for exposing the fisheye lens, we use "dot" elements, where at each dot the *e* beam is held at a different dwell time and is blanked when moving from one dot to another. The dose ranges between 3.45 pC and 10.65 pC. For the Bragg mirror, we use "curved elements" exposed with a step size of 20 nm and a dose of 3.5 $\mu C/cm^2$. After the dry-etching process, we scan the thickness of the residual Si of each feature (characterized by a specific dose) with an AFM and extract the contrast curve so that each dose is correlated with a residual thickness of Si. The contrast curve is shown in Fig. 2(b).

For the dry-etching process, we use an inductively coupled plasma (ICP) system. The ICP is fitted with two radio-frequency (rf) power supplies. The main power supply, the coil power, controls the intensity of the plasma, while the secondary power supply, the bias power, controls the ion energy of the ion flux to the etched substrate. The feed gases oxygen (O_2), sulfur hexafluoride (SF_6), and tetrafluoromethane (CF_4) are used at flow rates regulated using mass flow controllers. The pressure in the etch chamber is controlled by a throttle valve, which is continuously adjusted to keep the pressure constant during the etching process.

The etching parameters—the flow rates, coil power, bias power, and pressure—are all adjusted in order to have optimal conditions to transfer the SU-8 pattern into the Si film, with regard to etching anisotropy, etching selectivity, and surface roughness. For efficient transfer of the SU-8 pattern into the Si and to ensure a continuous profile and high fidelity in the transfer, we aim at a 1:1 etching selectivity of resist SU-8 versus silicon. In addition to the etching selectivity, control of the etching anisotropy in the Si is important for the optimal pattern transfer, especially for the Bragg mirror pattern, which is exposed and etched within the same stage as the fisheye lens and requires anisotropic etching. It is observed that the bias power has the largest effect on the anisotropy of the etch process. Increased bias power improves the etching anisotropy due to higher ion energy and thus improved directionality of the etching. However, increased bias also increases the surface roughness. A bias power value of 20 W with a coil power of 300 W is found to be a good compromise between anisotropy and roughness. Pressure also influences the etching anisotropy, and a weak interaction between bias power and pressure is evident. At higher pressures, the etching is more isotropic due to the reduction of the mean free path in the plasma and hence reduced ion energy and directionality. A pressure value of 10 mTorr is used in our process in order to obtain the optimal etching anisotropy (a steeper side-wall profile in the Bragg mirror). These values of bias and pressure lead to a low etching rate (180 nm per minute), which is not an important consideration in the development of the process.

The determination of the flow of the gases is found to be extremely important in order to meet the above requirements. We use the following rates: SF_6 (12 sccm, where "sccm" denotes standard cubic centimeter per minute) CF_4 (45 sccm), and O_2 (40 sccm). The flow rate of oxygen needs to be high enough to maintain the etching rate of the SU-8 close to the etching rate of the Si. If the flow rate

of the oxygen is too low (high), then the etching rate of the Si is much higher (lower) than the etching rate of the SU-8. This can be explained by the fact that the oxygen interacts with fluor in the chamber and reduces the fluor concentration in the chamber. Too low a flow of CF_4 leads to some deposition that accumulates on the surface and therefore increases the roughness. In addition to that, the Si etching rate in this case is much faster than the SU-8 etching rate. The same occurs when the flow of the CF_4 is too high, because in this case too much fluorine introduced into the plasma increases the etching rate of the Si. Therefore, an intermediate flow rate value of CF_4 needs to be fixed in order to have reasonable selectivity between the Si and the SU-8 etching rate.

The flow rate of the SF_6 is also significant in the process. Small amounts of SF_6 can greatly increase the plasma etching rate of the SU-8 over that obtained with a pure O_2 or O_2/Ar plasma, which etches SU-8 only very slowly. Even a small percentage of fluorinated gas can bring about a large increase in the removal rate for many resists, for two main reasons. First, fluorine atomic reactions produce reactive sites on the polymer backbone. Second, small amounts of fluorine increase the concentration of atomic oxygen in the plasma. However, the flow of SF_6 must not be too high in order to avoid a high etching rate of Si compared to that of the SU-8.

Residues composed of carbon, oxide, fluorine, and antimony are found on the substrate after the etching process. The source of the carbon and the oxygen could be the polymer layer and/or the etching gases and their products. Residues of fluorine can only come from the gas inserted into the chamber. However, antimony is an ingredient of the light-active component of SU-8. Antimony can build both volatile and nonvolatile components. With the presence of O^- and OH^- radicals in the plasma, nonvolatile $SbOF_3$ is formed. With the presence of fluorine in the plasma, the antimony forms the volatile molecule SbF_3. The amount of antimony accumulated at the surface could be reduced by increasing the formation of volatile byproducts, which means adding SF_6 to the plasma, directly lowering the surface roughness. However, we avoid increasing the SF_6 flow in order to obtain the optimal etching rate selectivity as mentioned above. Therefore, we have to compromise slightly with regard to the residues on the substrate.

[1] E. Acosta, D. Vazquez, L. Garner, and G. Smith, Tomographic method for measurement of the gradient refractive index of the crystalline lens. I. The spherical fishlens, J. Opt. Soc. Am. A **22**, 424 (2005).

[2] H. Lv and A. Liu, Research on coupling efficiencies of ball lenses, Opt. Precision Eng. **14**, 386 (2006).

[3] D. T. Moore, Gradient-index optics: A review, Appl. Opt. **19**, 1035 (1980).

[4] J. C. Maxwell, On the general laws of optical instruments, Q. J. Pure Appl. Math. **2**, 233 (1854).

[5] J. C. Maxwell, Problems, Cambridge Dublin Math. J. **8**, 188 (1854).

[6] U. Leonhardt, Perfect imaging without negative refraction, New J. Phys. **11**, 093040 (2009).

[7] N. Kundtz and D. R. Smith, Extreme-angle broadband metamaterial lens, Nat. Mat. **9**, 129 (2010).

[8] D. R. Smith, Y. Urzhumov, N. B. Kundtz, and N. I. Landy, Enhancing imaging systems using transformation optics, Opt. Express **18**, 21238 (2010).

[9] V. N. Smolyaninova, I. I. Smolyaninov, A. V. Kildishev, and V. M. Shalaev, Maxwell fisheye and Eaton lenses emulated by microdroplets, Opt. Lett. **35**, 3396 (2010).

[10] T. Zentgraf, Y. Liu, M. H. Mikkelsen, J. Valentine, and X. Zhang, Plasmonic Luneburg and Eaton lenses, Nat. Nanotechnol. **6**, 151 (2011).

[11] A. Di Falco, S. C. Kehr, and U. Leonhardt, Luneburg lens in silicon photonics, Opt. Express **19**, 5156 (2011).

[12] A. J. Danner, T. Tyc, and U. Leonhardt, Controlling birefringence in dielectrics, Nat. Photon. **5**, 35 (2011).

[13] T. Tyc, L. Herzánová, M. Šarbort, and K. Bering, Absolute instruments and perfect imaging in geometrical optics, New J. Phys. **13**, 115004 (2011).

[14] W. S. Jagger, The optics of the spherical fish lens, Vision Res. **32**, 1271 (1992).

[15] M. Born and E. Wolf, *Principles of Optics* (Cambridge University Press, Cambridge, 1999).

[16] T. Tyc and A. J. Danner, Absolute optical instruments, classical superintegrability, and separability of the Hamilton-Jacobi equation, Phys. Rev. A **96**, 053838 (2017).

[17] U. Leonhardt, S. Sahebdivan, A. Kogan, and T. Tyc, A simple model explaining super-resolution in absolute optical instruments, New J. Phys. **17**, 053007 (2015).

[18] U. Leonhardt and S. Sahebdivan, Theory of Maxwell's fisheye with mutually interacting sources and drains, Phys. Rev. A **92**, 053848 (2015).

[19] J. Perczel, P. Komar, and M. D. Lukin, Quantum Optics in Maxwell's Fish Eye Lens with Single Atoms and Photons, Phys. Rev. A **98**, 033803 (2018).

[20] Y. Koike and Y. Ohtsuka, in *Technical Digest, Topical Meeting on Gradient Index Optical Imaging Systems*, Palermo, Italy (1985), paper H1.

[21] Y. Koike, Y. Sumi, and Y. Ohtsuka, Spherical gradient index sphere lens, Appl. Opt. **25**, 3356 (1986).

[22] Y. Koike, A. Kanemitsu, Y. Shioda, E. Nihei, and Y. Ohtsuka, Spherical gradient index polymer lens with low spherical aberration, Appl. Opt. **33**, 3394 (1994).

[23] S. Ilyas and M. Gal, Gradient refractive index planar microlens in Si using porous silicon, Appl. Phys. Lett. **89**, 211123 (2006).

[24] H. Lv, B. Shi, L. Guo, and A. Liu, Fabrication of Maxwell fish-eye spherical lenses and research on distribution profiles of gradient refractive index, J. Opt. Soc. Am. A **25**, 3 (2008).

[25] L. H. Gabrielli and M. Lipson, Transformation optics on a silicon platform, J. Opt. **13**, 024010 (2011).

[26] U. Leonhardt, Optical conformal mapping, Science **312**, 1777 (2006).

[27] L. Xu and H. Chen, Conformal transformation optics, Nat. Photon. **9**, 15 (2015).

[28] I. I. Smolyaninov, V. N. Smolyaninova, A. V. Kildishev, and V. M. Shalaev, Anisotropic Metamaterials Emulated by Tapered Waveguides: Application to Optical Cloaking, Phys. Rev. Lett. **102**, 213901 (2009).

[29] J. Li and J. B. Pendry, Hiding under the Carpet: A New Strategy for Cloaking, Phys. Rev. Lett. **101**, 203901 (2008).

[30] Z. Xiong, L. Xu, Y-D. Xu, and H. Chen, Broadband illusion optical devices based on conformal mappings, Front. Phys. **12**, 124202 (2017).

[31] L. Xu, H. Chen, T. Tyc, Y. Xie, and S. A. Cummer, Perfect conformal invisible device with feasible refractive indexes, Phys. Rev. B **93**, 041406(R) (2016).

[32] R. K. Luneburg, *Mathematical Theory of Optics* (University of California Press, Berkeley and Los Angeles, 1964).

[33] T. Needham, *Visual Complex Analysis* (Clarendon Press, Oxford, 2002).

[34] T. Tyc and X. Zhang, Forum optics: Perfect lenses in focus, Nature **480**, 42 (2011) and the papers cited in Ref. [18].

[35] J. C. Minano, J. Sanchez-Dehesa, J. C. Gonzalez, P. Benitez, D. Grabovickic, J. Carbonell, and H. Ahmadpanahi, Experimental evidence of super-resolution better than $\lambda/105$ with positive refraction, New J. Phys. **16**, 033015 (2014).

[36] L. D. Landau and E. M. Lifshitz, *Electrodynamics of Continuous Media* (Pergamon, Oxford, 1984).

[37] I. H. Malitson, Interspecimen comparison of the refractive index of fused silica, J. Opt. Soc. Am. **55**, 1205 (1965).

[38] D. F. Edwards and E. Ochoa, Infrared refractive indexes of silicon, Appl. Opt. **19**, 4130 (1980).

[39] G. Beadie, M. Brindza, R. A. Flynn, A. Rosenberg, and J. S. Shirk, Refractive index measurements of poly(methyl methacrylate) (PMMA) from 0.4–1.6 μm, Appl. Opt. **54**, F139 (2015).